Measurement of $H \to b\bar{b}$ in Associated Production with the CMS Detector

by

Daniel Robert Abercrombie

B.S., Pennsylvania State University (2014)

Submitted to the Department of Physics
in partial fulfillment of the requirements for the degree of

Doctor of Philosophy

at the

MASSACHUSETTS INSTITUTE OF TECHNOLOGY

September 2020

Author . . . .

Department of Physics

June 30, 2020

Certified by . . . .

Christoph M. E. Paus

Professor of Physics

Thesis Supervisor

Accepted by . . . .

Nergis Mavalvala

Associate Department Head, Physics

Measurement of $H \to b\bar{b}$ in Associated Production with the CMS Detector

by

Daniel Robert Abercrombie

Submitted to the Department of Physics
on June 30, 2020, in partial fulfillment of the
requirements for the degree of
Doctor of Philosophy

Abstract

We measured $VH \to b\bar{b}$ with the CMS Detector.

Thesis Supervisor: Christoph M. E. Paus
Title: Professor of Physics

Acknowledgments

Thanks.

Contents

Chapter 1

Introduction

One of the most curious features of physics at small scales, which will likely frustrate students for the rest of time, is that certain sequences of events only have a probability of happening. There is no guarantee that an electron and a positron approaching each other at high energies will annihilate and produce an muon and an anti-muon. However, this event might still occur at a later time at with the exact same initial conditions. Furthermore, the observation of resonances where this is more likely to happen when the electron and positron approach each other at particular speeds does not mean that a Z boson was present in a given interaction. It just means that the weak component of the electroweak force significantly increases the probability of the muonic final state, given the total energy of the initial state. The sum of probabilities from different possible field interactions with particular initial conditions is the only thing we can measure. This is also only possible when observing many events with the same initial conditions.

This point is difficult to convey concisely, so many laypeople, as well as some practicing physicists, are confused by the terminology adopted by the field. But this distinction is relevant to the topic of this work. This document presents a measurement of a cross section. Cross section is the name given to the probability of an interaction occurring. Reported cross sections can be split up to describe different contributions to final states, and they can be collated into what are called “production cross sections” which describe the probabilities of particular intermediate states "occurring" (even though intermediate states never exist in reality).

The main point is that if there exists some interesting particle, and it interacts with other particles, you can see an increased probability of certain initial states resulting in certain final states. This can teach the observer about the role of the interesting particle, without ever directly seeing it.

1.1 Measurement of the Higgs Cross Section

The purpose of the following document is to present the methods and results of measuring the strength of the coupling between the Higgs Boson and bottom quarks. In this context, the Higgs Boson makes up one of the previously mentioned intermediate states that cannot be shown as present in a given event. The cross section measurement relies on a number of physics processes that will be accounted for in this document.

To measure this coupling, the Higgs Boson must first be "produced" before measuring its coupling strength to bottom quarks. Since we are not technologically advanced enough to achieve this generation using bottom quarks directly, we use measured Higgs generation rates from normal constituents of protons. We constrain ourselves further by requiring that the Higgs is generated by associated production.

After the Higgs is generated, it can decay into a number of different particles. This work is only concerned with one kind of decay.

The math that this all relies on is presented in Chapter 2.

1.2 Motivation for the Measurement

This is Thomas Kuhn's "normal science".

Precision measurements are needed to be certain of what we think.

Precision measurements often lead to discrepancies that are explained by a fundamental shift in the model.

The Standard Model is a good one. It will not be fully replaced, but at worst expanded upon. Just like Newton's Laws are still a reasonable approximation for General Relativity, The Standard Model is a good approximation for most things we have been able to interact with so far.

The only lingering questions are Dark Matter and Dark Energy, but there is no reason to assume that precise measurements of known phenomena will not lead to an explanation.

1.3 Historic Context

First, we have The Standard Model.

Parts were proven correct by the observation of the weak bosons.

The Higgs was observed in 2013.

The Higgs decaying to $b\bar{b}$was observed in 2018. [3]

1.4 Using the CMS Detector

The CMS detector is a general purpose detector used to make many observations of conditions unattainable on Earth outside of the LHC.

It has many stationary parts, and a couple of moving ones too.

This device is described in detail in Chapter 3.

Chapter 2

Theory

Before diving into the description of the experimental apparatus, an explanation of why it is expected to work is needed. There are many textbooks that cover the Standard Model, as there are many students who study it. Much of what follows is taken from the book by Mark Thompson [11].

The Standard Model Lagrangian can be defined as a sum of Lagrangians that each describe the interactions between different fermions and bosons. Equations of motion can be extracted from a Lagrangian $\mathcal{L}$ for a particle field ϕ_i using the Euler-Lagrange equations.

$$\delta_\mu \left(\frac{\delta \mathcal{L}}{\delta(\delta_\mu \phi_i)} \right) - \frac{\delta \mathcal{L}}{\delta \phi_i} = 0 \tag{2.1}$$

In the measurement of $H \to b\bar{b}$ in associated production, many components of the Standard Model are of interest. These will be introduced as needed. First, I will give a brief explanation of Higgs field's non-zero vacuum energy, a trait that makes the Higgs one of the central keystones to Standard Model. After that, the electroweak Lagrangian will be described since the cross section of associated production depends on the coupling of the Higgs Boson to the W and Z vector bosons. The coupling of the electroweak force to fermions is also important to understand both the generation of these intermediate states and the resulting final state that the CMS detector records.

Another important factor for this work is a the decay of the Higgs boson itself into bottom quarks. This depends on the Higgs directly coupling to fermions. Finally, we will briefly consider the part of the Lagrangian describing the strong force. Since the LHC is a hadron collider, understanding of the strong force is required to extract data from LHC collisions.

2.1 The Higgs Mechanism

In both of these components of the Standard Model Lagrangian, the Higgs coupling actually gives the vector bosons and massive fermions their mass [5, 7, 8]. (In this work, neutrinos can be treated as massless.) The granting of mass happens for two reasons: the Higgs field has a non-zero vacuum expectation value, and the Higgs field couples to vector boson and massive fermion fields.

The Higgs can be described as two complex scalar fields in a weak isospin doublet with a quartic potential. The Lagrangian for a free Higgs is then

$$\mathcal{L} = (\delta_\mu \phi)^\dagger (\delta^\mu \phi) - (\mu^2 (\phi^\dagger \phi) + \lambda (\phi^\dagger \phi)^2) \tag{2.2}$$

Through the virial theorem, the potential has a minimum value when

$$\phi^\dagger \phi = \frac{-\mu^2}{2\lambda} = \frac{v^2}{2} \tag{2.3}$$

This potential of the Higgs field breaks the SU(2) $\times$ U(1) symmetry of the Standard Model Lagrangian. Through this non-zero vacuum expectation value, the Higgs then has a constant influence in other parts of the Standard Model Lagrangian. For this measurement, three interactions that the Higgs makes with this influence need to be considered: the Higgs interacting with itself, the Higgs interacting with the electroweak vector bosons, and the Higgs interacting with quarks.

The first two interactions manifest in the Lagrangian when we force the SU(2) $\times$ U(1) symmetry on the Lagrangian in Equation (2.2). The derivatives must be replaced.

$$\delta_\mu \to D_\mu = \delta_\mu + i\frac{g_W}{2}\boldsymbol{\sigma} \cdot \mathbf{W}_\mu + ig'\frac{Y}{2}B_\mu \tag{2.4}$$

ϕ can be rewritten to satisfy the vacuum expectation value in the gauge that will give us the massless neutral boson known as a photon.

$$\phi(x) = \frac{1}{\sqrt{2}}\begin{pmatrix} 0 \\ v + h(x) \end{pmatrix} \tag{2.5}$$

This leads to the following expansion for the kinetic term of the Lagrangian.

$$\begin{aligned}(D_\mu\phi)^\dagger(D^\mu\phi) =& \frac{1}{2}(\delta_\mu h)(\delta^\mu h) + \frac{1}{8}g_W^2(W_\mu^{(1)} + iW_\mu^{(2)})(W^{(1)\mu} - iW^{(2)\mu})(v+h)^2 \\ &+ \frac{1}{8}(g_W W_\mu^{(3)} - g'B_\mu)(g_W W^{((3)\mu} - g'B^\mu)(v+h)^2\end{aligned} \tag{2.6}$$

Terms that are quadratic in terms of the gauge boson fields reveal the mass of the fields. Taking $h(x) \to 0$, the terms for $W^{(1)}$ and $W^{(2)}$ are the just

$$\frac{1}{4}g_W^2 v^2 W_\mu^{(1)} W^{(1)\mu} \quad \text{and} \quad \frac{1}{4}g_W^2 v^2 W_\mu^{(2)} W^{(2)\mu},$$

giving the mass.

$$m_W = \frac{1}{2}g_W v \tag{2.7}$$

The quadratic terms for $W^{(3)}$ and B mix to give a non-diagonal mass matrix $\mathbf{M}$.

$$\frac{v^2}{8}\begin{pmatrix} W_\mu^{(3)} & B_\mu \end{pmatrix} \mathbf{M} \begin{pmatrix} W^{(3)\mu} \\ B^\mu \end{pmatrix} = \frac{v^2}{8}\begin{pmatrix} W_\mu^{(3)} & B_\mu \end{pmatrix} \begin{pmatrix} g_W^2 & -g_W g' \\ -g_W g' & g'^2 \end{pmatrix} \begin{pmatrix} W^{(3)\mu} \\ B^\mu \end{pmatrix} \tag{2.8}$$

The non-diagonal matrix allow $W^{(3)}$ and B to mix. Physical states must be represented by a diagonal Hamiltonian. Diagonalizing the term above gives masses of the physical states.

$$\frac{1}{8}v^2 \begin{pmatrix} A_\mu & Z_\mu \end{pmatrix} \begin{pmatrix} 0 & 0 \\ 0 & g_W^2 + g'^2 \end{pmatrix} \begin{pmatrix} A^\mu \\ Z^\mu \end{pmatrix} = \frac{1}{2} \begin{pmatrix} A_\mu & Z_\mu \end{pmatrix} \begin{pmatrix} m_A^2 & 0 \\ 0 & m_Z^2 \end{pmatrix} \begin{pmatrix} A^\mu \\ Z^\mu \end{pmatrix} \tag{2.9}$$

This gives us the masses of the neutral gauge bosons.

$$m_A = 0 \quad \text{and} \quad m_Z = \frac{1}{2}v\sqrt{g_W^2 + g'^2} \tag{2.10}$$

From the simple act of requiring SU(2) × U(1) symmetry on the Lagrangian of a scalar doublet with non-zero vacuum expectation value, the masses of all the electroweak gauge bosons have been produced.

2.2 Associated Production

The next thing to consider is the couplings also produced by this process. The couplings will allow us to determine more precisely the parameters above by measuring cross sections.

The physical states of W^+ and W^- bosons can be written as the raising and lowering operators for isospin.

$$W^\pm = \frac{1}{\sqrt{2}} \left(W^{(1)} \mp iW^{(2)} \right) \tag{2.11}$$

The second term of Equation (2.6) can be further expanded.

$$\frac{1}{4}g_W^2 W_\mu^- W^{+\mu}(v+h)^2 = \frac{1}{4}g_W^2 v^2 W_\mu^- W^{+\mu} + \frac{1}{2}g_W^2 v W_\mu^- W^{+\mu} h + \frac{1}{4}g_W^2 W_\mu^- W^{+\mu} h^2 \tag{2.12}$$

The second term on the right hand side of Equation (2.12) gives us the coupling strength of a vertex with a Higgs and two W bosons.

$$g_{HWW} = \frac{1}{2}g_W^2 v = g_W m_W \tag{2.13}$$

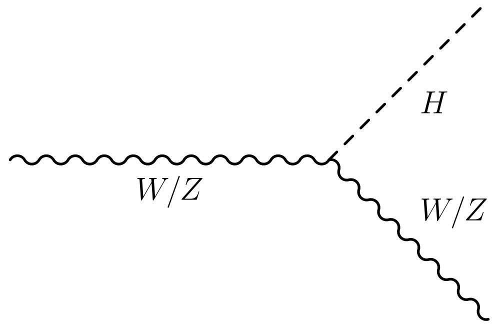

Figure 2-1: Above is the Feynman diagram for associated production. The W or Z boson radiates a Higgs boson. Both bosons later decay into particles detected by CMS.

The coupling to the Z boson can also be found from Equation (2.9) by substituting $(v+h)^2$ back in for v^2 and extracting the terms proportional to $hZ_\mu Z^\mu$.

$$g_{HZZ} = \frac{1}{2}\left(g_W^2 + g'^2\right) v = \sqrt{g_W^2 + g'^2} m_Z \tag{2.14}$$

When arranged in a way that the W or Z boson radiates the Higgs, as opposed to a Higgs decaying into a pair of W or Z bosons, the process is called associated production or *Higgstrahlung*. The vertex showing associated production is pictured in Figure 2-1.

2.2.1 Production Mechanisms of Vector Bosons

The W and Z bosons are themselves intermediate states, never existing in a directly observable manner. They must be produced through interacts with stable fermions. Since the LHC is a hadron collider, considering the vector bosons' couplings with quarks would be most relevant.

Quarks are fermions that couple to each other through the strong force, resulting from a SU(3) symmetry. There are three generations of quarks each consisting of a pair of quark types. Their mass eigenstates are denoted as down-type or up-type. Table 2.1 displays some of the characteristics of these quarks. A feature of quarks is that their mass eigenstates do not match their weak eigenstates. There is a mixing among the down-type quarks that is parametrized by the Cabibbo-Kobayashi-

Table 2.1: The quarks and some stuff about them.

	1st gen.	2nd gen.	3rd gen.	Q	$I_W^{(3)}$
down-type	d	s	b	$-\frac{1}{3}$	$-\frac{1}{2}$
up-type	u	c	t	$+\frac{2}{3}$	$+\frac{1}{2}$

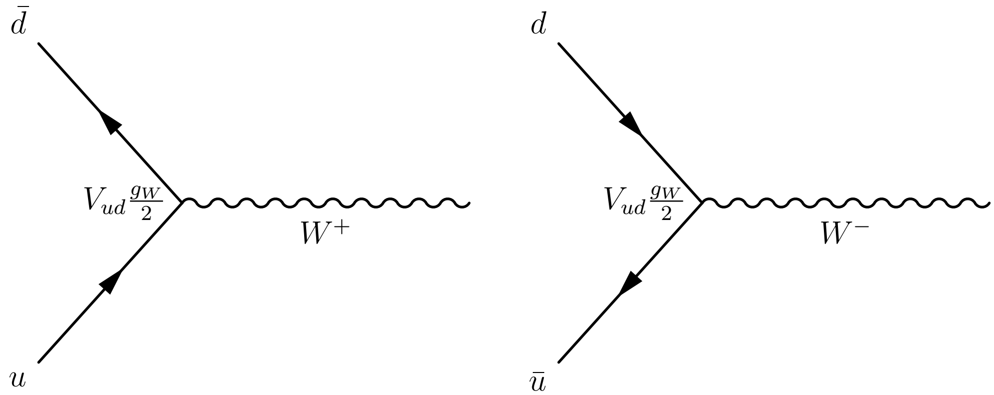

Figure 2-2: Above are diagrams for generating W^+ and W^- bosons. the u and d quarks in the diagram can be replaced with any up-type or down-type quark, respectively. The CKM matrix element would in the vertex element would be changed accordingly.

Maskawa (CKM) matrix.

$$\begin{pmatrix} d' \\ s' \\ b' \end{pmatrix} = \begin{pmatrix} V_{ud} & V_{us} & V_{ub} \\ V_{cd} & V_{cs} & V_{cb} \\ V_{td} & V_{ts} & V_{tb} \end{pmatrix} \begin{pmatrix} d \\ s \\ b \end{pmatrix} \tag{2.15}$$

The mass eigenstates are denoted as d, s, and b, while d', s', and b' are the weak eigenstates. This mixing allows quarks to change generations through interaction with $W^\pm$ bosons, which raise or lower the weak isospin. The following is the charge current vertex interaction.

$$-i\frac{g_W}{\sqrt{2}} \begin{pmatrix} \bar{u} & \bar{c} & \bar{t} \end{pmatrix} \gamma^\mu \frac{1}{2}(1-\gamma^5) \begin{pmatrix} V_{ud} & V_{us} & V_{ub} \\ V_{cd} & V_{cs} & V_{cb} \\ V_{td} & V_{ts} & V_{tb} \end{pmatrix} \begin{pmatrix} d \\ s \\ b \end{pmatrix}$$

The vertices for this interaction is shown in Figure 2-2 arranged in a way to show the processes of generating a W^+ or W^- boson from annihilating quarks. The γ

matrices in the interaction are present because the SU(2) component of the Standard Model only interacts with left-handed fermions and right-handed anti-fermions. For this reason, the SU(2) component is more accurately labelled $\mathrm{SU}(2)_L$. From Equation (2.11), the $W^{\pm}$ bosons are completely made up of the $W^{(1)}$ and $W^{(2)}$ components of the $\mathrm{SU}(2)_L$, so they also only interact with left-handed fermions and right-handed anti-fermions.

Both the photon and the Z boson mix the $\mathrm{SU}(2)_L$ and U(1) components of the Standard Model. Production of the Z needs to be directly understood for this measurement, but it is more straightforward to determine the strength of the Z couplings to left- and right-handed fermions by exploiting the symmetry of photon interactions. That is, the photon interacts the same with left and right handed charged fermions, and not at all with neutral fermions. This is shown directly with experiments with leptons. The charged leptons, electrons, muons, and taus, interact with photons, while the respective neutrinos do not. From the mixing in Equation (2.8), the photon and Z fields can be expressed as the following.

$$A_\mu = B_\mu \cos\theta_W + W_\mu^{(3)} \sin\theta_W \tag{2.16}$$

$$Z_\mu = -B_\mu \sin\theta_W + W_\mu^{(3)} \cos\theta_W \tag{2.17}$$

θ_W is known as the weak mixing angle. The relative strengths of the B and $W^{(3)}$ couplings are determined directly through lepton electro-magnetic characteristics, keeping in mind that $W^{(3)}$ only interacts with left handed particles. The following are the electro-magnetic interaction strengths of left- and right-handed electrons and neutrinos.

$$e_L: \qquad Qe = \frac{1}{2}g' Y_{e_L} \cos\theta_W - \frac{1}{2}g_W \sin\theta_W \tag{2.18}$$

$$\nu_L: \qquad 0 = \frac{1}{2}g' Y_{\nu_L} \cos\theta_W - \frac{1}{2}g_W \sin\theta_W \tag{2.19}$$

$$e_R: \qquad Qe = \frac{1}{2}g' Y_{e_R} \cos\theta_W \tag{2.20}$$

$$\nu_R: \qquad 0 = \frac{1}{2}g' Y_{\nu_R} \cos\theta_W \tag{2.21}$$

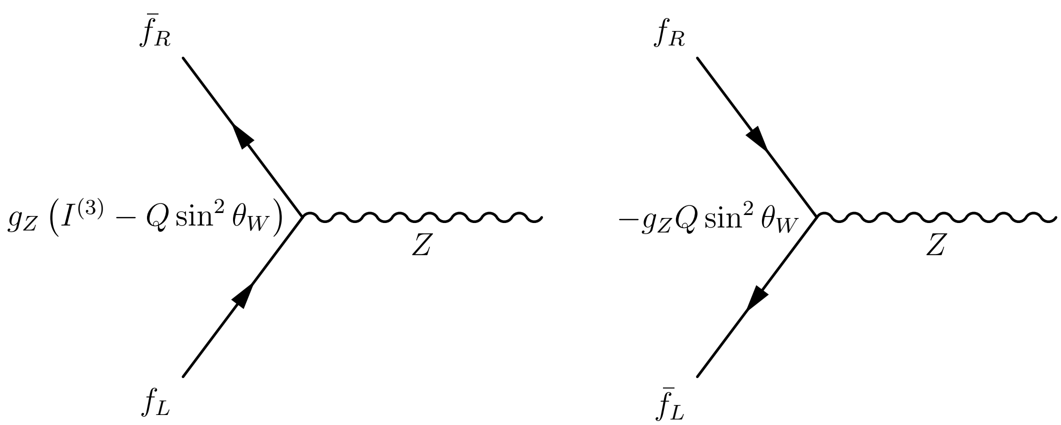

Figure 2-3: Above are diagrams for generating Z bosons. Left- and right-handed fermions are both coupled to, but with different coupling strengths.

Y_{e_L} and Y_{ν_L} must be equal to maintain $\mathrm{SU}(2)_L$ symmetry. To satisfy these contraints, the follow definition of Y is needed.

$$Y = 2\left(Q - I_W^{(3)}\right) \tag{2.22}$$

The following relationship also arises from these experimental constraints.

$$e = g_W \sin\theta_W = g' \cos\theta_W \tag{2.23}$$

Returning to the Z boson, from Equation (2.17), and defining

$$g_Z = \frac{e}{\sin\theta_W \cos\theta_W}, \tag{2.24}$$

we have the following couplings to left- and right-handed fermions.

$$\begin{aligned}-\frac{1}{2}g' \sin\theta_W (Y_{f_L}\bar{u}_L\gamma^\mu u_L + Y_{f_R}\bar{u}_R\gamma^\mu u_R) + I_W^{(3)} g_W \cos\theta_W\left(\bar{u}_L\gamma^\mu u_L\right) = \\ g_Z\left(\left(I^{(3)} - Q\sin^2\theta_W\right)\bar{u}_L\gamma^\mu u_L - Q\sin^2\theta_W \bar{u}_R\gamma^\mu u_R\right)\end{aligned} \tag{2.25}$$

Now the coupling of the Z to left- and right-handed quarks can be calculated from Table 2.1, remembering that $I_W^{(3)}$ for right-handed fermions is 0. Diagrams showing the interaction strengths of fermion-Z vertices are shown in Figure 2-3.

Thus vector bosons couple to quarks, the constituents of hadrons, which means they can be produced at the LHC. As mentioned earlier in this section, quarks interact through an SU(3) symmetry that results in the strong force. The three states that this symmetry supports are known as color states, and they are labelled red, green, and blue, or r, g, and b. The resulting gauge bosons are known as gluons, and they carry the following color states.

$$r\bar{g}, g\bar{r}, r\bar{b}, b\bar{r}, g\bar{b}, b\bar{g}, \frac{1}{\sqrt{2}}(r\bar{r} - g\bar{g})\text{and}\frac{1}{\sqrt{6}}(r\bar{r} + g\bar{g} - 2b\bar{b})$$

At low energy, the coupling constant for the strong force is on the order of unity. This leads to color confinement, so that quarks an appreciable distance apart do not interact with each other. To achieve this, all observable hadronic states are color singlets. The most common hadronic states are mesons, made of a quark/anti-quark pair with the color singlet state

$$\psi(q\bar{q}) = \frac{1}{\sqrt{3}}(r\bar{r} + g\bar{g} + b\bar{b}), \tag{2.26}$$

and baryons, made of three quarks with the following color singlet state.

$$\psi(qqq) = \frac{1}{\sqrt{6}}(rgb - rbg + gbrgrb + brg - bgr) \tag{2.27}$$

Baryons can also be composed of three anti-quarks, which has a state corresponding to Equation (2.27), but with anti-color.

For this measurement, protons are collided at the LHC. The proton consists of two u quarks, and one d quark. Since the three quarks inside the proton interact strongly, there are also many virtual gluons and quark/anti-quark pairs present at all times. The quantity and energies of all these partons are not able to be calculated since QCD is non-perturbative. They can be measured in deep inelastic scattering experiements though. In these, electrons are scattered off of protons, and parton distribution functions (PDFs) can be measured. The PDFs for protons are shown in Figure 2-4.

From these things, we can predict the cross section of generating W and Z bosons

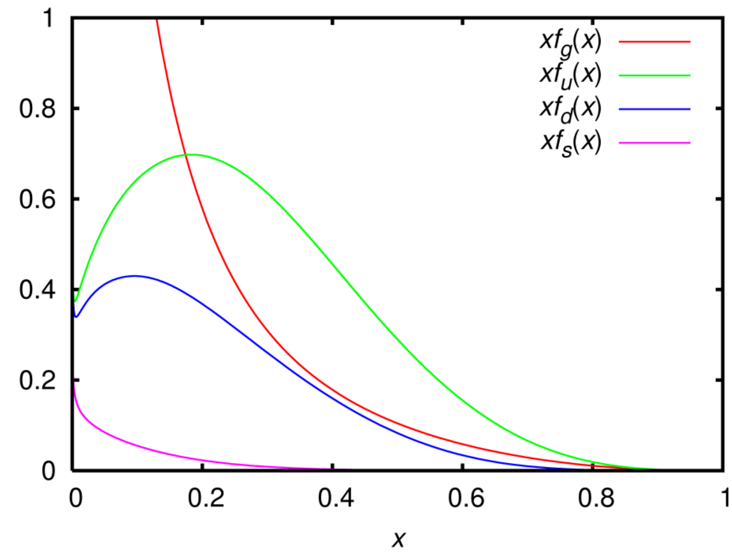

Figure 2-4: The P.D.F.

at the LHC. These need to be very massive though, since they're going to radiate a Higgs. This complicates the calculation a bit.

2.2.2 Decay Channels of Vector Bosons

Due to the couplings described in Section 2.2.1, the vector bosons decay into quarks. However, in the hadronic environment produced at the LHC these are not the best indicators of a vector boson intermediate state. This measurement uses leptonic decays in the final state since the contributions of the vector boson intermediate states to leptonic final states of appropriate kinematics are larger compared to other contributions to this final state.

There are three generations of leptons. Each generation consists of a charged lepton, and a neutral neutrino. The left-handed charged lepton and neutrino of each generation form an electroweak SU(2) doublet. In order of increasing mass, the three generations are called electron, muon, and tau. Heavier charged leptons decay into lighter leptons via the weak force. Two neutrinos result from this decay, as shown in Figure 2-5, making the characteristics of the parent lepton's parent difficult to reconstruct. The tau lepton has enough mass to consistently decay before reaching the CMS detector. The tau lepton is also massive enough to also decay into quarks,

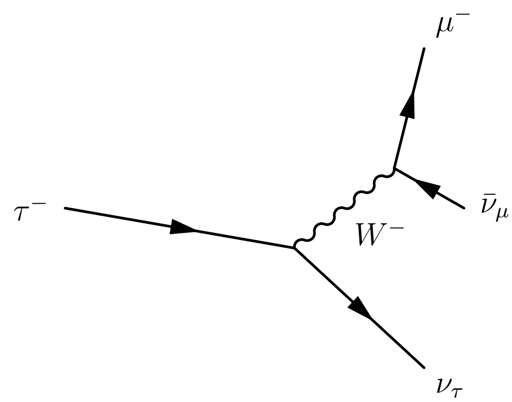

Figure 2-5: Heavier leptons can decay to lighter leptons while emitting two neutrinos. Above is an example of a decay of $\tau \to \nu_\tau \mu \bar{\nu}_\mu$. The neutrinos cannot be measured at CMS, so it is better to avoid such decays in the analysis.

making its measurement even more complicated. Muons have an average lifetime long enough to penetrate the entire detector, and electrons are stable particles. As a result, only muons and electrons are considered in this analysis. The Feynman diagrams for the decay channels of interest are shown in Figure 2-6.

2.3 Decay Channels of the Higgs

What we are ultimately interested in measuring is the contribution of the Higgs intermediate state to the final state of $b\bar{b}$. Since the Higgs is a SU$(2)_L$ doublet of scalar fields, the term $-g_f(\bar{L}\phi R + \bar{R}\phi^\dagger L)$ in the Standard Model Lagrangian is invariant under SU$(2)_L\times$ SU$(1)_Y$, where L is a left-handed fermion doublet, and R is a right-handed singlet. If the Higgs doublet is expanded around the vacuum expectation value, as Equation (2.5), the Lagrangian term becomes the following.

$$\mathcal{L}_f = -\frac{g_f}{\sqrt{2}} v \left(\bar{f}_L f_R + \bar{f}_R f_L\right) - \frac{g_f}{\sqrt{2}} h \left(\bar{f}_L f_R + \bar{f}_R f_L\right) \tag{2.28}$$

In Equation (2.28), f refers to the lower field of the fermion's SU$(2)_L$ doublet. The Lagrangian also includes terms for the upper field since the conjugate of ϕ has the same symmetries as ϕ.

The Lagrangian showing fermion-Higgs interactions in Equation (2.28) consists of two terms. Since v is constant, the first term would be consistent with a fermion's

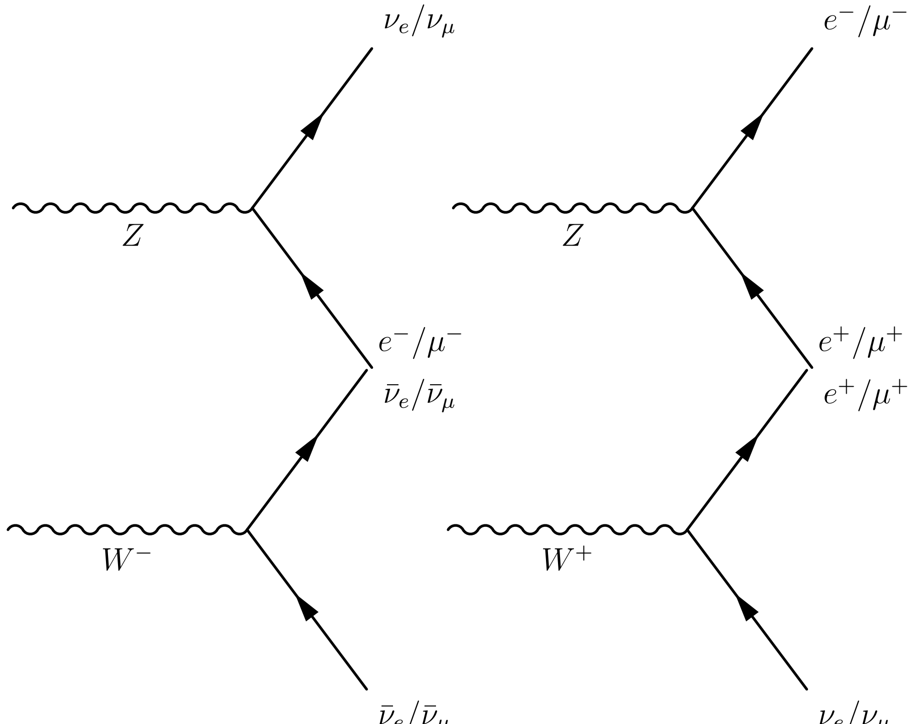

Figure 2-6: Above are the three different vector boson decays we are interested in.

mass, assuming an appropriate coupling constant.

$$g_f = \sqrt{2}\frac{m_f}{v} \tag{2.29}$$

The second term is the coupling of the fermion to the Higgs field with the same coupling constant. This is the mechanism by which the Higgs give fermions their masses, and also why the Higgs couples more strongly to massive particles. The Feynman rule for the interaction vertex between the Higgs and fermions is proportional to the fermion's mass. Of the quarks, the b quark is the second most massive. The most massive t quark is too massive to be the final decay product of an on-shell Higgs. In fact, the predicted branching ratio of $H \to b\bar{b}$ is 57.8%. Therefore, measuring $H \to b\bar{b}$ is the most direct measurement to confirm this theory of quark masses. The diagram for this decay can be combined with the Feynman diagrams in Figure 2-1, Figure 2-2 or 2-3, and one of the decays in Figure 2-6 in order to generate the full Feynman diagrams for the processes being measured in this analysis. One such full diagram is shown in Figure 2-7.

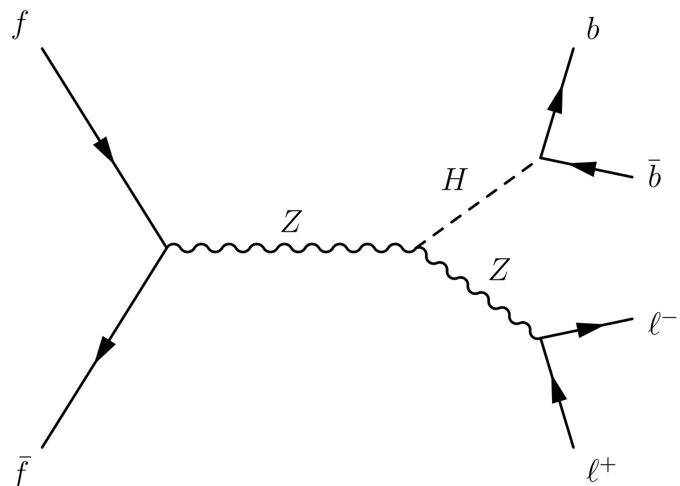

Figure 2-7: Above is the full Feynman diagram for $ZH \to \ell^+\ell^- b\bar{b}$.

2.4 Other Relevant Standard Model Processes

There are other processes that must be acknowledged in order to explain how the CMS detector works. I'll fill those in as needed?

Chapter 3

The CMS Detector

The Compact Muon Solenoid (CMS) detector, located at the LHC, consists of multiple sub-detectors. Ideally, time could be saved for the dedicated reader by only detailing the parts of the detector that are relevant for the analysis presented in this work. Unfortunately, a characteristic of hadron collider measurements is that almost all sub-systems of the detector are used to make the final measurement.

A brief overview of all the detector subsystems are therefore presented in this chapter. More can be learned about the design and motivations for the detector in the TDR [2]. Information presented on the CMS design parameters are taken directly from that document unless otherwise noted.

3.1 Associated Production at the LHC

The CMS detector only observes events. Before describing the devices that are used to observe and record events, the method of generating interesting events must be described. The CMS detector is located at the Large Hadron Collider (LHC). Described in detail in multiple publications [6], a brief description is given here.

The LHC, with a circumference of 26.7 km, is large enough to be considered located in multiple towns and countries, but it will suffice to say it is near Geneva, Switzerland at the European Organization for Nuclear Research (CERN), the main campus of which is addressed in Meyrin, Switzerland. This campus itself also spans the border between Switzerland and France. This large circumference is needed since charged particles traveling in a circular path with radius r emit synchrotron radiation at the following rate.

$$P = \frac{q^2 p^4}{6\pi\epsilon_0 m^4 c^5 r^2} \tag{3.1}$$

The amount of power lost by the particles decreases quadratically with the size of the collider. In addition, the energy lost decreases with the mass of the accelerated particles to the fourth power. The LHC was built in the same tunnels that were used for LEP, which was a collider for electrons and positrons that took much of its data at $\sqrt{s} = 98\,\text{GeV}$. The resulting LHC is designed to collide protons at energies of $\sqrt{s} = 14\,\text{TeV}$, with the data for this analysis taken at $13\,\text{TeV}$.

Though Figure 2-4 showed that not all of the energy from each proton goes into the interaction, there still is adequate phase space available to generate the massive off-shell vector bosons that are needed for *Higgstrahlung*, via the mechanisms described in Section 2.2.1.

The removal of a quark from one proton and an anti-quark from the other leads to two non-color-singlet states in close proximity to each other. The resulting spray of hadronic particles generated from the vacuum to restore color singlets are called jets. The detectors are designed to distinguish these jets from more interesting decay products in the interaction.

In order to generate a large amount of data needed for measurements like associated production, the LHC operates at a high frequency of collisions. For Run 2, there is a proton bunch crossing every 25 ns. The CMS detector must be able to read out and process data on that timescale.

3.2 Detector Requirements

One configuration of possible final state particles is shown in Figure 2-7. There, two oppositely charged leptons and two b quarks are the end decay products. The b quarks also hadronize form color singlets well before reaching the detector, but the resulting jets can actually be distinguished well from the jets resulting from the fragmenting protons.

Hadrons containing b quarks decay through the weak force since they require a flavor change. As mentioned before, the CKM matrix in Equation 2.15 quantifies the mixing between the different quark flavors. The value of V_{tb} is close to unity, and since the CKM matrix is unitary, V_{cb} and V_{ub} are small. This means the matrix element weak decays of the b hadrons is small. This is the only decay channel available to the lightest b hadrons, so their lifetimes are relatively long. The delayed decay results in a jet with a secondary vertex where many of its particles are generated from the vacuum at a distance from the initial collision point.

Alternate signatures of interest can be seen by substituting other vector boson final states from Figure 2-6. In these, there may be one or zero charged leptons, with one or two neutral leptons, respectively. Neutral particles are difficult to detect, with neutral leptons being capable of passing through the entire Earth without being part of a detectable interaction. The CMS detector therefore ignores the neutrinos, but their presence can still be inferred. Even with the variation in momentum along the beam direction, all partons in each proton have approximately zero momentum in the transverse direction. Therefore, the sum of the transverse momenta of all final state particles must also be zero. Many events in CMS have an overall imbalance in the transverse plane. This imbalance is labelled Missing Transverse Energy, E_T^{miss}, or MET. Large MET in an event is often a sign of high energy neutrinos that the detector cannot detect.

We need to identify all of these interesting particles, as well as be able to reconstruct missing transverse momentum. In addition, the additional hadronic activity in the event, called pileup, must be mitigated. The energy of the decay products have energies on the scale of the masses of the parent particles. The detector must be capable of measuring jets and leptons with energies on the order of 10s or 100s of GeV. Better energy resolution for each of these decay products allows better separation of our signal process from background processes that generate very similar final states.

3.3 Detector Design

The CMS detector as a whole has cylindrical symmetry around the beam access. It is 21 meters long and 15 meters in diameter. There are gaps at either end to allow the beam, but otherwise tries to cover the full solid angle around the collision point. The azimuthal angle of a particle relative to the beam axis is described by pseudorapidity, η.

$$\eta = -\ln\left[\tan\left(\frac{\theta}{2}\right)\right] \tag{3.2}$$

The barrel portion of CMS can detect particles with $|\eta| < 2.4$, while the forward caps of the detector can reach $|\eta| < 5.0$.

Different technologies are better for measuring the energy or other kinematics variables of different particles. As a result, the CMS detector is made up of different sub-detector systems, arranged in cylindrical layers.

The innermost layer is designed to extrapolate the tracks of charged particles back to their point of origin. This is called the Silicon Pixel Detector. The next layer is designed to measure the energies of photons and electrons. The third layer measures the energies of both charged and neutral hadrons. Outside of these three layers is a superconducting solenoid, which generates a magnetic field for the entire detector. On the very outside of the detector are gas chambers designed to detect muons interspersed with the iron return yoke for the solenoid. A slice of the CMS detector showing the relative positions of each layer is shown in Figure 3-1.

The magnet is described first since the magnetic field it produces is a key part of most of the rest of the detector. After that, the sub-detectors are summarized in the order of closest to farthest from the beamline, since this is the order that particles would interact with the layers.

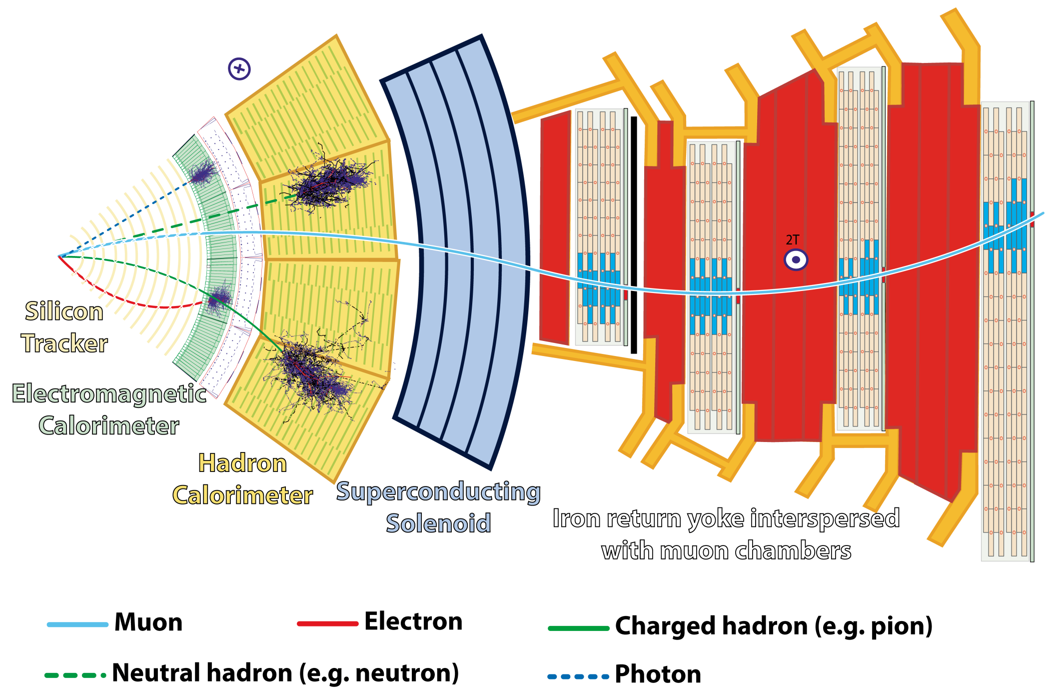

Figure 3-1: A slice of the CMS detector is shown above [1]. The four detector layers are labelled and show the penetration depths of various particles stable enough to travel a measureable distance.

3.3.1 Solenoid Magnet

Part of the CMS acronym acknowledges the role of the solenoid magnet. The presence of a magnetic field is necessary for accurate measurements of charged particles passing through the silicon pixel detector and muon chambers.

The magnetic field generated is designed to cause the path of a muon with 1 TeV of energy to bend enough to have a momentum resolution of 10%. Inside the solenoid, the magnetic field reaches 4 T, with a return field that is large enough to cause muon tracks to curve throughout the muon chambers outside the magnet.

A super-conducting solenoid enables the creation of a magnetic field with the required strength. A current of 19.5 kA is sent through 2168 turns over 12.9 m. The magnetic field stores 2.7 GJ of energy. In order to hold this, the structural components holding the magnet and the detector in place are strong enough to withstand 64 atm of hoop pressure.

3.3.2 Silicon Pixel Detector

The layer closest to the beamline is designed to obtain a precise track pointing to the orgin of particles passing into the detector. It is made up of layers of many small pixels to do this. As distance from the interaction point increases, the pixel size also increases.

The innermost three layers, with the closest layer being a distance of $r = 4\,\text{cm}$ from the interaction point, are made of hybrid pixel detectors. Each pixel has dimensions of $100 \times 150\,\mu\text{m}$. At this size, only one out of every ten thousand inner layer pixels is triggered in a typical LHC bunch crossing. Outside of the pixel detector layers, silicon strip detectors are used. These are placed in the region that is $20 < r < 55\,\text{cm}$ from the beamline. Strip dimensions give a cell size of approximately $10\,\text{cm} \times 80\,\mu\text{m}$. 2–3% of cells are activiated during a typical bunch crossing. The outermost layers are made of larger strips with cell sizes of $25\,\text{cm} \times 180\,\mu\text{m}$. About 1% of these pixels are triggered each bunch crossing.

The active material of the silicon pixel detector is semi-conducting silicon. When charged particles pass through, electron-hole pairs are generated and drift apart due to a bias voltage. The voltage change when these pairs reach their respective electrodes indicates a charged particle passed through. Because of this, the silicon pixel detector cannot detect any neutral particles, but it gives a point of origin for charged particles that is accurate enough to identify pileup.

3.3.3 Electromagnetic Calorimeter

The next layer of the detector is called the Electromagnetic Calorimeter or ECAL. This layer is designed to fully capture and measure the energy of photons and electrons. The ECAL is made of crystals of the scintillating material Lead Tungstate ($PbWO_4$). Each crystal is placed in the detector so that its smallest face is facing the collision point. These small faces have dimensions of $22 \times 22\,\text{mm}$. The length of each crystal is 230 mm, and the far face is slightly larger at $26 \times 26\,\text{mm}$. $PbWO_4$ has a radiation length of $\chi_0 = 8.9\,\text{mm}$ and a Moliere radius of 21 mm. This means each crystal is 25.8 radiation lengths, containing the full shower within the ECAL, and each shower is also localized to within one crystal from the initial ionization.

The scintillating properties of $PbWO_4$ are also desireable for observing LHC collisions. 4.5 photons for every MeV of deposited energy are ultimately detected by the photo-multipliers at the far end of the crystals. This is a low number for most experiments, but the only photons and electrons of interest in this measurement deposit at least 10s of GeV of energy. This gives the ECAL energy resolutions in the range of $5 - 10\%$. More importantly, the scintillation is very fast. 80% of the light from an interaction is emitted within the 25 ns between bunch crossings, making it easy to associate the readouts with the appropriate collision.

3.3.4 Hadronic Calorimeter

The Hadronic Calorimeter (HCAL) has the same goal as the ECAL, where it contains particles and measures the energy emitted by them. However, it tries to do this for hadrons, such as protons, neutrons, and stable mesons. Since they are all much more massive than electrons, the ionizing collisions in a typical scintillator does not slow them down enough to contain them.

3.3.5 Muon Chambers

(MuCham)

3.4 Detector Performance

Is okay

3.4.1 Test Beam Performance

Very nice

3.4.2 Trigger

warning

3.4.3 Online Calibration

uses lasers

3.5 Data Format

ROOT files

3.5.1 Event Reconstruction

???

3.5.2 Offline Calibration

POGs

3.6 Accessing Data

XRootD

Chapter 4

Simulation

4.1 Backgrounds to the Analysis

In order to effectively measure Higgs production, we need to be able to accurately estimate other events that end up in our selection.

4.2 Event Generation

We use different generators.

Details in Appendix D.

4.2.1 Tree Level Simulation

4.2.2 Parton Showers

4.3 Detector Simulation

4.4 Corrections to Simulation

4.4.1 Smearing

Muons

Electrons

Jets

4.4.2 Selection Efficiencies

4.4.3 Control Regions

Light Flavor Jets

Heavy Flavor Jets

$t\bar{t}$

Chapter 5

Event Selection

5.1 Object Definitions

Section 3.5.1 describes how detector responses are linked to possible physical particles. We want to remove false positives, so here are some tighter requirements for counting for event selection.

Once we have our objects defined, we can count them.

5.1.1 Muons

Muons can show up in weakly decaying jets, so we're only interested in isolated ones here.

5.1.2 Electrons

Electrons do the same thing as muons, but messier because the ECAL isn't as clean as the muon chambers.

5.1.3 Jets

Jets are messier still.

Pileup removal is a big deal here.

5.1.4 MET

MET is corrected.

5.1.5 Undesirable Particles

There are certain particles that we do not want present. We make very loose selections for those and veto on them.

Photons

Tau Leptons

5.2 Removal of QCD

We have some cuts across the board on our objects in order to remove events that are just QCD.

5.3 Categories of Vector Boson Decay

Now that we are ready to count, we can count leptons in order to characterise potential vector bosons.

5.3.1 0 Leptons

5.3.2 1 Lepton

5.3.3 2 Leptons

5.4 Topology of Higgs Decay

5.4.1 Resolved Jets

We reconstruct two b jets.

5.4.2 Boosted Jet

When the Higgs has very high p_T, the jet clustering algorithms can find both daughter particles as being part of a single jet.

Chapter 6

Analysis Results

6.1 Systematic Uncertainties

6.2 Combination Fit Method

6.3 Results

Chapter 7

Conclusions

Appendix A

Detector Projects

Each collaborator must contribute to the operation of the CMS detector before his or her name is added to the author list. The operation of the detector is distinct from analyzing the data generated by the detector, so all collaborators must adopt some role outside of being a physicist.

This appendix details projects I completed in order to contribute to the operation of the CMS detector. The first project presented is the Dynamo Consistency project. It is a plugin for the dynamic data management system Dynamo [9] that compares the inventory of files Dynamo expects at a site with the files that are actually at a site. The other project described is known as Workflow Web Tools. This is a dynamic web server that displays errors reported by the CMS computing infrastructure to operators, and allows those operators to perform corrective actions through the web page. Workflow Web Tools also tracks operator actions for future use in training various machine learning models. Both projects produced software packages written in Python [12,13] and available through the Python Package Index (PyPI) as `dynamo-consistency` and `workflowwebtools`.

A.1 Dynamo Consistency

[4] [10]

A.2 Workflow Web Tools

Appendix B

Physics Calculations

Appendix C

Data Format

Appendix D

Generator Parameters

Appendix E

Data Card

Bibliography

[1] David Barney. CMS Detector Slice. CMS Collection., Jan 2016.

[2] The CMS Collaboration. *CMS Physics: Technical Design Report Volume 1: Detector Performance and Software*. Technical Design Report CMS. CERN, Geneva, 2006.

[3] The CMS Collaboration. Observation of higgs boson decay to bottom quarks. *Physical Review Letters*, 121(12), Sep 2018.

[4] Alvise Dorigo, Peter Elmer, Fabrizio Furano, and Andrew Hanushevsky. Xrootd-a highly scalable architecture for data access. *WSEAS Transactions on Computers*, 1(4.3):348–353, 2005.

[5] F. Englert and R. Brout. Broken symmetry and the mass of gauge vector mesons. *Phys. Rev. Lett.*, 13:321–323, Aug 1964.

[6] Lyndon Evans and Philip Bryant. LHC machine. *Journal of Instrumentation*, 3(08):S08001–S08001, aug 2008.

[7] G. S. Guralnik, C. R. Hagen, and T. W. B. Kibble. Global conservation laws and massless particles. *Phys. Rev. Lett.*, 13:585–587, Nov 1964.

[8] Peter W. Higgs. Broken symmetries and the masses of gauge bosons. *Phys. Rev. Lett.*, 13:508–509, Oct 1964.

[9] Yutaro Iiyama, Benedikt Maier, Daniel Abercrombie, Maxim Goncharov, and Christoph Paus. Dynamo – handling scientific data across sites and storage media, 2020.

[10] Erwin Laure, A Edlund, F Pacini, P Buncic, M Barroso, A Di Meglio, F Prelz, A Frohner, O Mulmo, A Krenek, et al. Programming the grid with glite. Technical report, CERN, Geneva, Switzerland, 2006.

[11] Mark Thomson. *Modern particle physics*. Cambridge University Press, Cambridge, 2013.

[12] Guido Van Rossum and Fred L. Drake. *Python 3 Reference Manual*. CreateSpace, Scotts Valley, CA, 2009.

[13] Guido Van Rossum and Fred L Drake Jr. *Python reference manual*. Centrum voor Wiskunde en Informatica Amsterdam, 1995.